PLEASE CITE THIS ARTICLE AS DOI: 10.1116/6.0003320

Thickness Dependent Thermal Conductivity of Strontium Titanate (SrTiO₃) Thin Films on Silicon (Si) Substrate

Roshan Sameer Annam^a Swapneel Danayat^a Avinash Nayal^a Fatema Tarannum^a Matthew Chrysler^b Joseph Ngai^b Jiechao Jiang^c Aaron J Schmidt^d Jivtesh Garg^a

- a. School of Aerospace and Mechanical Engineering, University of Oklahoma, Norman, OK-73019, USA
- b. Department of Physics, University of Texas-Arlington, Arlington, TX-76010, USA
- Department of Materials Science & Engineering, University of Texas-Arlington, Arlington, TX-76010, USA
- d. Fourier Scientific LLC

Electronic mail: garg@ou.edu

Abstract: Perovskite materials, of which strontium titanate (STO) and its thin films are an example, have attracted significant scientific interest, due to their desirable properties and the potential to tune thermal conductivity, by employing several techniques. Notably, strontium titanate thin films on silicon (Si) substrates serve as a fundamental platform for integrating various oxides onto Si substrates, making it crucial to understand the thermal properties of STO on Si. This work investigates the thermal conductivity of STO thin films on Si substrate for varying film thickness (12nm, 50nm, 80 nm, and 200 nm) at room temperature (~300 K). The thin films were deposited using Molecular Beam Epitaxy (MBE) on Si substrate and their thermal conductivity is characterized using Frequency Domain Thermoreflectance (FDTR) method. The measured values ranged from 7.4±0.74 for the 200 nm thick film to 0.8±0.1 Wm⁻¹K⁻¹ for the 12 nm thick film, showing a large effect of the film thickness on the thermal conductivity values. The trend of the This is the author's peer reviewed, accepted manuscript. However, the online version of record will be different from this version once it has been copyedited and typeset.

PLEASE CITE THIS ARTICLE AS DOI: 10.1116/6.0003320

values is diminishing with the corresponding decrease in the thin film thickness, with a reduction of 38% to 93% in the thermal conductivity values, for film thicknesses from 200 nm to 12 nm. This reduction in the values is relative to the bulk single crystal values of STO which may range from 11 to 13.5 Wm⁻¹K⁻¹, as measured by our FDTR-based experiment. The study also explores the evaluation of volumetric heat capacity (C_p). The measured volumetric heat capacity for the 200 nm thin film is 3.07 MJm⁻³K⁻¹, in reasonable agreement with the values available in the literature.

I. Introduction

The ability to control thermal conductivity is important for a wide range of applications. For instance, advancements in both oxide thermal barrier coatings and thermoelectric materials hinge on engineering a thermally resistive material that is optimized in conjunction with other parameters such as thermal expansion, microstructure, toughness, or carrier mobility. Similarly, materials with high thermal conductivity are desirable for thermal management applications. The remarkable ability of perovskites to accommodate a wide range of materials opens avenues to tune material properties through an appropriate choice of elements³. In recent years, epitaxial growth of complex oxides with the perovskite crystal structure has figured prominently in studies of the physics of correlated electrons⁴ and in the search for electronic materials for information technology and sensing^{5,6}. Measurement of thermal conductivity of epitaxial thin films is another way to characterize the quality of epitaxial films, beside x-ray diffraction (XRD)⁷, transmission electron microscopy (TEM)^{8,9}, and in situ reflection high energy electron diffraction (RHEED)¹⁰. The perovskite family of oxides shows promise for thermal barrier¹¹ and thermoelectric applications¹²-¹⁵, because of its compositional tunability, which is accompanied by high-temperature stability. One such material from the perovskite family is strontium titanate (Fig. 1) and its epitaxial thin

PLEASE CITE THIS ARTICLE AS DOI: 10.1116/6.0003320

films have attracted interest as possible insulating layers in dynamic random-access memories^{16–18}, ferroelectric thin film structures¹⁹ and high-Tc superconductor devices^{20,21}.

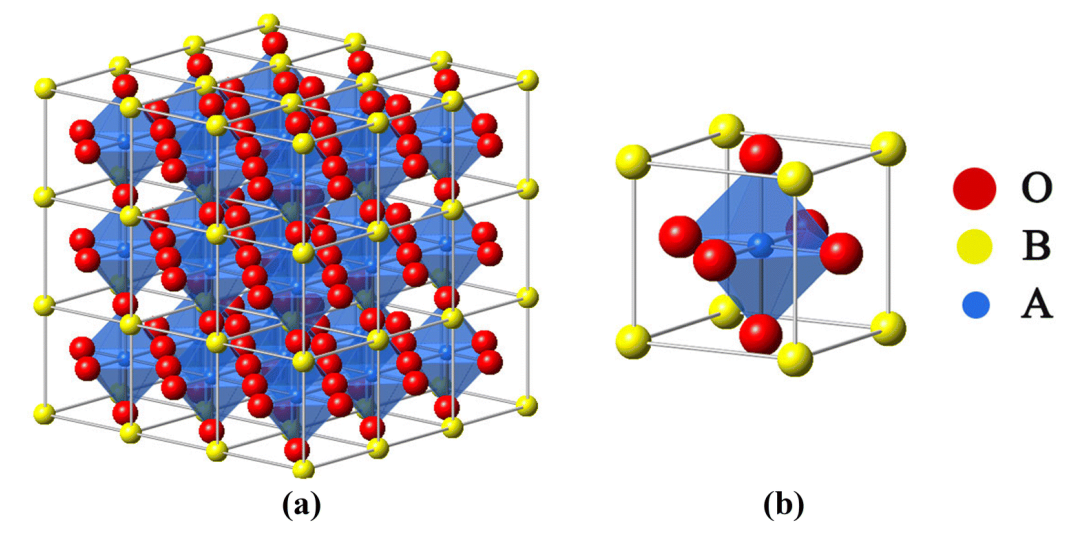


FIG 1. a) STO crystal structure and b) unit cell

Due to its potential applications, it is important to investigate thermal conductivity properties of STO and tunability of thermal conductivity using techniques such as varying domain size^{22–28}, defects, doping, deposition using different techniques under varying growth conditions and deposition of films on different substrates. Computational methods have also been applied to understand the thermal transport in STO.

With respect to thermal conductivity measurements for STO thin films, Oh *et al.* measured STO thin films produced using MBE and PLD (Pulsed Laser Deposition) techniques on single-crystalline STO and LSAT (LaAlO₃)_{0.3}(Sr₂AlTaO₆)_{0.7}) substrates²⁹. The STO film thickness across all the samples was in the range of 300 to 400nm. The thermal conductivity of all the samples at 300 K ranged from ~ 9 to 12 Wm⁻¹K⁻¹ for MBE samples while *k* values were in the range of ~ 4 to 12 Wm⁻¹K⁻¹ for PLD samples²⁹.

PLEASE CITE THIS ARTICLE AS DOI: 10.1116/6.0003320

of ~ 4 to 1 Wm⁻¹K⁻¹ at 275 K³².

Sarantopoulos et al. demonstrated that STO thin films grown on DyScO₃ substrate under tensile strain showed a significant reduction in thermal conductivity at room temperature to ~2.5 Wm⁻¹K⁻ 1, when compared to the STO on LSAT and STO substrates (~6 Wm⁻¹K⁻¹)³⁰. Katsufuji et al. measured thermal conductivity of two samples where one of them was a thin film of 70 nm SrVO₃ on STO and the other samples was thin film of 30 nm SrVO₃ and 30nm SrTiO₃ on LSAT substrates with thermal conductivities of 8 Wm⁻¹K⁻¹ and 2 Wm⁻¹K⁻¹ respectively³¹. Bugallo et al. measured SrTiO₃- LaCoO₃ superlattices on STO substrate, with varying periodicity of SrTiO₃ - LaCoO₃ and a total thickness of 80nm. The combinations of SrTiO₃ - LaCoO₃ were 40x2, 20x4, 10x8, 8x10, 5x16, 4x20 and 2x40 where the first number is the thickness of each layer and the other is the repetition of each layer. The thermal conductivity values for all the combinations were in the range

Kumar et al. investigated the effect of Nb, and oxygen vacancies on thermal conductivity and thermoelectric properties of STO thin films. The lattice thermal conductivity at 300 K was measured to be 2.2 W/mK and the thermoelectric figure of merit was around 0.29 at 1000 K. The thin films were deposited on SiO₂/Si and LAO (LaAlO₃) substrates³³. Yu et al. in their study measured the thermal conductivity of oxygen deficient lanthanum-doped STO thin films Sr_{1-x}La_xTiO_{3-δ}, deposited on STO/Si substrates, with the film thickness being ~10 nm. The measured thermal conductivity of the thin film at 300 K was around 3 W/mK, which represents a large reduction in the value in comparison to bulk single crystal STO (~11 Wm⁻¹K⁻¹)¹. Foley et al. looked at the thermal conductivity of nano grained STO thin films deposited on Sapphire substrates. Thin films with a thickness of 170 nm with varying grain sizes were deposited using a chemical deposition process. There was a reduction of 50%-60% across the grain sizes, as

PLEASE CITE THIS ARTICLE AS DOI: 10.1116/6.0003320

compared to the bulk values. A reduction in thermal conductivity with decreasing grain size was also observed in this work³⁴.

Brooks et al. demonstrated the ability to tune the thermal conductivity of homoepitaxial STO thin films using MBE by varying deposition parameters such as growth temperature, oxidation temperature and cation stoichiometry. The study showed a 80% reduction in thermal conductivity from 11.5 Wm⁻¹K⁻¹ for stoichiometric STO to 2 Wm⁻¹K⁻¹ by creating strontium rich homoepitaxial $Sr_{1+\delta}TiO_x$ films and also by introducing planar defects such as the (SrO)₂ Ruddlesden-Popper planar defects³. Breckenfeld et al. deposited SrTiO₃ thin films using PLD on NdGaO₃, where they illustrated that films with excess Sr displayed drastic reduction in thermal conductivity, as compared to films with excess Ti³⁵. Zhang et al. in their study of tunability of STO thermal conductivity, used annealing treatments as an effective method to induce reduction in the thermal conductivity values³⁶. Wiedigen *et al.* induced defects (as a function of the deposition process), lattice strain (due to film-substrate lattice mismatch) and studied their effect on the film thermal conductivity in homoepitaxial STO films, produced by ion-beam sputtering³⁷.

Computational studies on the lattice thermal conductivity of SrTiO₃ were conducted by Fumega et al. using both ab initio Molecular Dynamic simulations and Density Functional Theory. This study focuses on the effect of structural distortions on the thermal conductivity of STO, by identifying key features of thermal transport in STO and the changes they undergo under a particular case of structural distortions. The thermal conductivity of bulk single crystal STO is measured to be 13.4 Wm⁻¹K⁻¹². Martelli et al. conducted studies on the thermal conductivity of doped and undoped STO, over a temperature range of 2 to 400 K and identified different heat flow regimes. In one of the regimes for undoped STO the thermal conductivity increased faster than T³,

PLEASE CITE THIS ARTICLE AS DOI: 10.1116/6.0003320

at low temperatures, an effect that was attributed to hydrodynamic phonon transport. Such an effect was lost with the introduction of any dopant³⁸.

Data on thermal conductivity of STO thin films on Si substrate is lacking. STO on Si substrate serves as an epitaxial platform upon which other multifunctional oxides can be integrated for various device applications³⁹. Understanding thermal transport of this material system is important to such applications⁴⁰. In this study, we examine the thermal conductivity of four STO thin films of thicknesses of 12 nm, 50 nm, 80 nm, and 200 nm deposited on Si substrates.

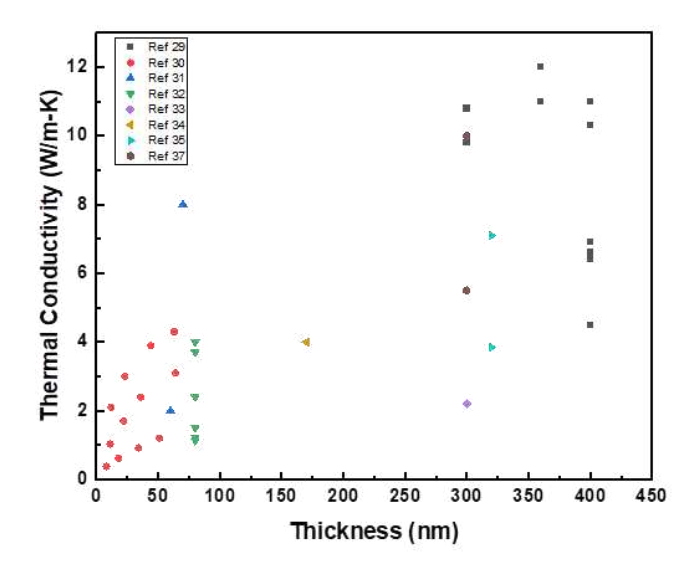


FIG 2. Plot showing the values of thermal conductivity of STO based thin films for various growth conditions and substrates.

II. Sample Preparation:

The STO thin films were epitaxially grown on 2" diameter, undoped Si (100) wafers (Virginia Semiconductor) using oxide molecular beam epitaxy (MBE). Epitaxial growth was initiated through the crystallization of 2 unit-cells of amorphous STO deposited at room temperature, as discussed in detail elsewhere⁴¹. After crystallization of this seed-layer at ~ 500 °C in ultra-high

PLEASE CITE THIS ARTICLE AS DOI: 10.1116/6.0003320

vacuum, subsequent layers were grown through co-deposition of SrO and TiO₂ fluxes on Si wafers held at a temperature of 580 °C in a background pressure of 3×10^{-7} Torr of O₂. After growth, each wafer was diced (Disco DAD3220) into smaller pieces measuring 6×4 mm² for thermal conductivity measurements.

III. Structural Characterization:

X-ray diffraction (XRD) confirms the epitaxial quality of the STO thin films on Si. The XRD measurements were taken on a Bruker D-8 system that is equipped with a standard Cu k α x-ray source ($\lambda = 1.54056$ Å). Figure 3 shows survey scans of the 4 films with the various diffraction peaks labelled. The out-of-plane lattice constants of the 12 nm, 50 nm, 80 nm, and 200 nm films were 3.918 Å, 3.924 Å, 3.898 Å, and 3.910 Å, respectively, which largely compares well with the bulk lattice constant of STO (3.905 Å).

IV. Experimental Setup:

Thermal conductivity measurements were performed using the frequency domain thermoreflectance method (FDTR). A sinusoidally modulated pump laser (wavelength λ = 473 nm) with a power of 51.41 mW was used to create a periodic heat source at the sample surface. The frequency range for the modulation of the pump laser is from 2000 Hz to 50 MHz. A probe laser (λ = 532 nm) was used to measure the change in phase of the temperature response of the surface with respect to the phase of the input heat signal. This is achieved by measuring the surface temperature through a measurement of the reflected probe beam's intensity which is dependent on the surface temperature of gold transducer layer through a thermoreflectance coefficient. The measured phase lag is fitted to an analytical 2D heat conduction model, by varying parameters such as material thermal conductivity.

PLEASE CITE THIS ARTICLE AS DOI: 10.1116/6.0003320

Si (004) Kα SrTiO₃ Silicon Si (002) STO (002) Intensity (Arb. Units) Si (004) Kβ 12 nm 50 nm STO 80 nm (003) STO (001) 200 nm 50 60 70 80 20 30 40 2θ (deg.)

FIG 3. X-ray diffraction of the four SrTiO₃ films showing epitaxial growth on silicon. Various diffraction peaks are labeled.

The values of the parameters corresponding to best fit yield the material properties. The four STO samples of varying thicknesses (200nm, 80nm, 50nm, 12nm) were coated with ~130 nm of gold film, which acts as a transducer layer, absorbing heat from the pump beam, and conducting the heat into the sample. With the gold coating, these materials become a 3-layer stacking problem, which can be visualized in Fig. 4.

PLEASE CITE THIS ARTICLE AS DOI: 10.1116/6.0003320

Au $[C_{p} \quad k_{\perp} \quad k_{\parallel} \quad d]$ STO thin film $[C_{p} \quad k_{\perp} \quad k_{\parallel} \quad d]$ $[C_{p} \quad k_{\perp} \quad k_{\parallel} \quad d]$ Si Substrate

FIG 4. Multilayer stack model for Strontium Titanate (STO) thin film on Si Substrate Each layer, starting from the top layer of gold to the Si substrate, is characterized by volum

Each layer, starting from the top layer of gold to the Si substrate, is characterized by volumetric heat capacity (C_P), cross-plane thermal conductivity (k_\perp), in-plane thermal conductivity (k_\parallel), and thickness. Thermal boundary conductance (TBC) of Au/STO thin film interface (G_1) and STO thin film/Si substrate interface (G_2), are also shown in the figure. For a n layer system, the number of properties associated with the system are 5n-1 resulting in 14 parameters for a 3-layer material system. By eliminating the parameters with known values (such as silicon thermal conductivity), the number of unknown parameters to be obtained by the fitting process between measured and computed phase lag are reduced. Another important parameter for the fitting analysis is the laser spot size. The laser spot size determines the size of the heat source on the sample surface, which is an important parameter used in the calculation of the phase lag using the 2D heat conduction model. The estimate of these parameters is described next.

V. Methodology:

Transducer is a device which converts one form of energy to another. In our case, the Au thin film converts the energy from the laser to create a periodic heat source at the sample's surface. The periodicity of the heat source corresponds to the frequency at which the pump laser beam is

PLEASE CITE THIS ARTICLE AS DOI: 10.1116/6.0003320

modulated. The Au film is deposited using a pellet (99% purity) as a target, for the deposition 42-44 purchased from Kurt. J Lesker Company. We use Lesker Nano36 Evaporator thermal evaporator, (part of Microfabrication Research & Education Center at University of Oklahoma) to deposit ~100nm of gold film, which is a target thickness set in the thermal evaporator machine as a process parameter. The final gold film thickness achieved will be different, as it is based on the position of the sample placed on the sample holder. Before the start of the gold film deposition process, the STO samples were mounted on the sample stage in the thermal evaporator, where a piece of sapphire reference sample was placed in between 200 and 50 nm STO samples, and another in between 80 and 12 nm STO samples respectively.

The thermal conductivity, thickness and CTR (coefficient of thermoreflectance) values for Au layer deposited on the STO samples are determined by performing transducer layer characterization using a reference sample, with known thermal properties such as fused silica or

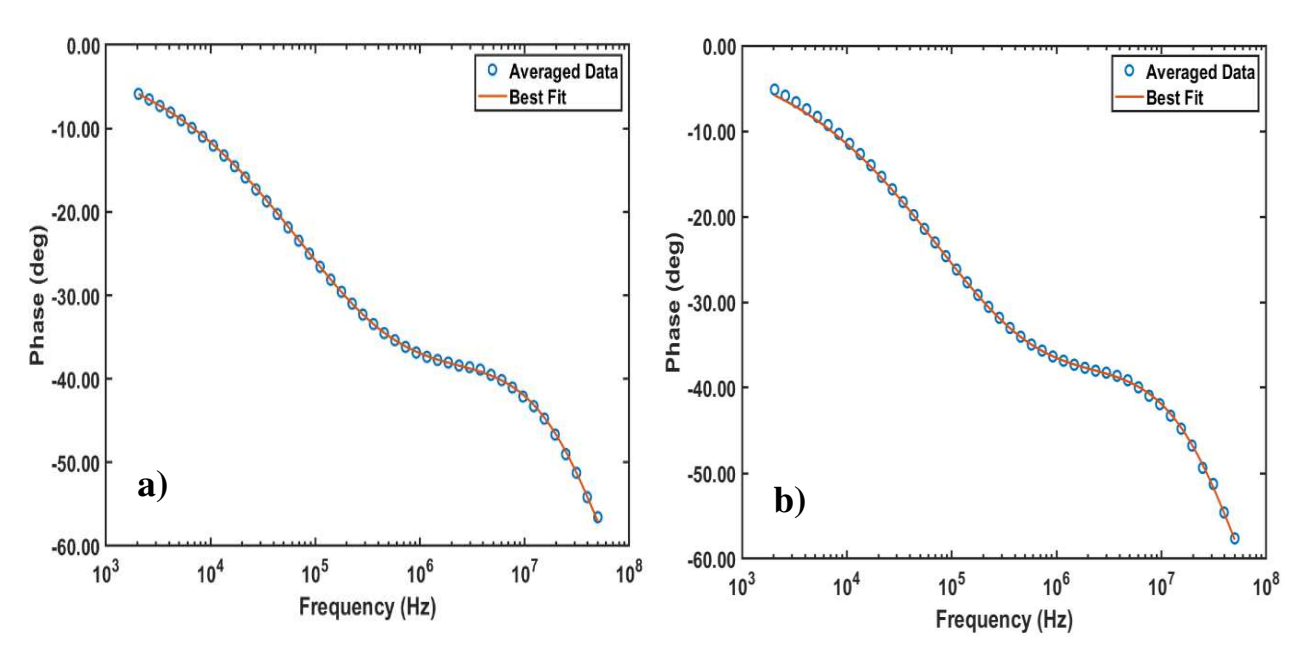


FIG 5. Curve fit analysis for transducer (Au thin film) on sapphire reference samples for a) 200 and 50 nm STO samples b) 80 and 12 nm STO samples, determining the thermal conductivity and thickness properties of Au thin film on the STO samples (used as input parameters for STO analysis)

PLEASE CITE THIS ARTICLE AS DOI: 10.1116/6.0003320

sapphire⁴⁵. By fitting the thermal properties of the transducer layer on reference samples, we use these values as input parameters for the analysis of the STO samples. Such transference of properties of gold layer from reference sample to STO samples is possible because of the assumption in the analysis methodology that the values of the properties of the Au layer, for samples placed very close to each other will be the same. The properties of the sapphire reference sample, chosen for the transducer layer characterization analysis, are pre-determined in the analysis software. The C_P and cross-plane k values for the reference sample used in this process are 3.066 MJm⁻³K⁻¹ and 36.43 Wm⁻¹K⁻¹ respectively. Since the reference sample is a c axis sapphire, we use anisotropy (k_{\parallel} / k_{\perp}) value to be 0.85.

Based on this, Table. 1 compiles the results for the Au layer properties for reference sapphire samples, used in the analysis of the STO samples. The value of C_p (also pre-determined in the fitting analysis software) for gold is 2.484 MJm⁻³K⁻¹ ⁴⁶.

Figs. 5 a) and b) are the best curve fit figures for the transducer layer analysis of reference sapphire samples for 200 and 50 nm STO samples, and 80 and 12 nm STO samples respectively. Since the 200 and 500 nm samples share the same sapphire reference sample, the reference sample curve fit analysis is represented by the same figure for both the samples. This is also true for the 80 and 12 nm STO samples. We observe that the best curve fit line for the measured data fits near perfectly for both the measurements. This indicates the fitted values of the thermal conductivity and the thickness for the transducer layer, determined during this analysis is the correct solution. The following table is the properties of the Au thin film, which are used in the analysis of the STO samples.

TABLE I. Au thin film transducer layer characterization using properties of reference sample

STO thin film thickness	$k (\mathrm{Wm}^{-1}\mathrm{K}^{-1})$	Au Film thickness t (nm)
200 nm	196±25.48	137±9.59
80 nm	196±25.48	138±9.66
50 nm	196±25.48	137±9.59
12 nm	196±25.48	138±9.66

The SrTiO₃ thickness is measured as a function of the deposition rate, which is computed from the rates of SrO and TiO₂ fluxes, which are measured and controlled during the STO thin film deposition process. Volumetric heat capacity values for Au and Si layers are taken from the literature.

$$C_{\rm p} = a + bT + \frac{c}{T^2} + \frac{d}{\sqrt{T}} \tag{1}$$

The volumetric heat capacity (Jmol⁻¹K⁻¹) for STO is calculated using the above formula mentioned in the literature^{47,48}, where the values of a, b, c, and d, are 134.581 Jmol⁻¹K⁻¹, 0.0045567 Jmol⁻¹K⁻², 11.979e⁵ Jmol⁻¹K, and -414 Jmol⁻¹K^{-1/2} respectively. Using a molecular weight of 189.49 gmol⁻¹ and a density of 4.81 gcm⁻³ for strontium titanate, the volumetric heat capacity is obtained to be 2.77 MJm⁻³K⁻¹. Experimentally, the volumetric heat capacity of STO was determined to be around 2.78 MJm⁻³K⁻¹ ⁴⁹.

VI. Results and Discussion:

A. Thermal conductivity analysis

PLEASE CITE THIS ARTICLE AS DOI: 10.1116/6.0003320

In Figs. 6 a, b, c, d, the slope of the phase lag plot and its best fit curve in the mid to high-frequency range changes from a trough to a slight crest as the sample thickness decreases (indicated in Fig. 6 using red highlighted box). This discernible difference in the phase lag plots indicates that all the samples with varying thickness exhibit discrete trends.

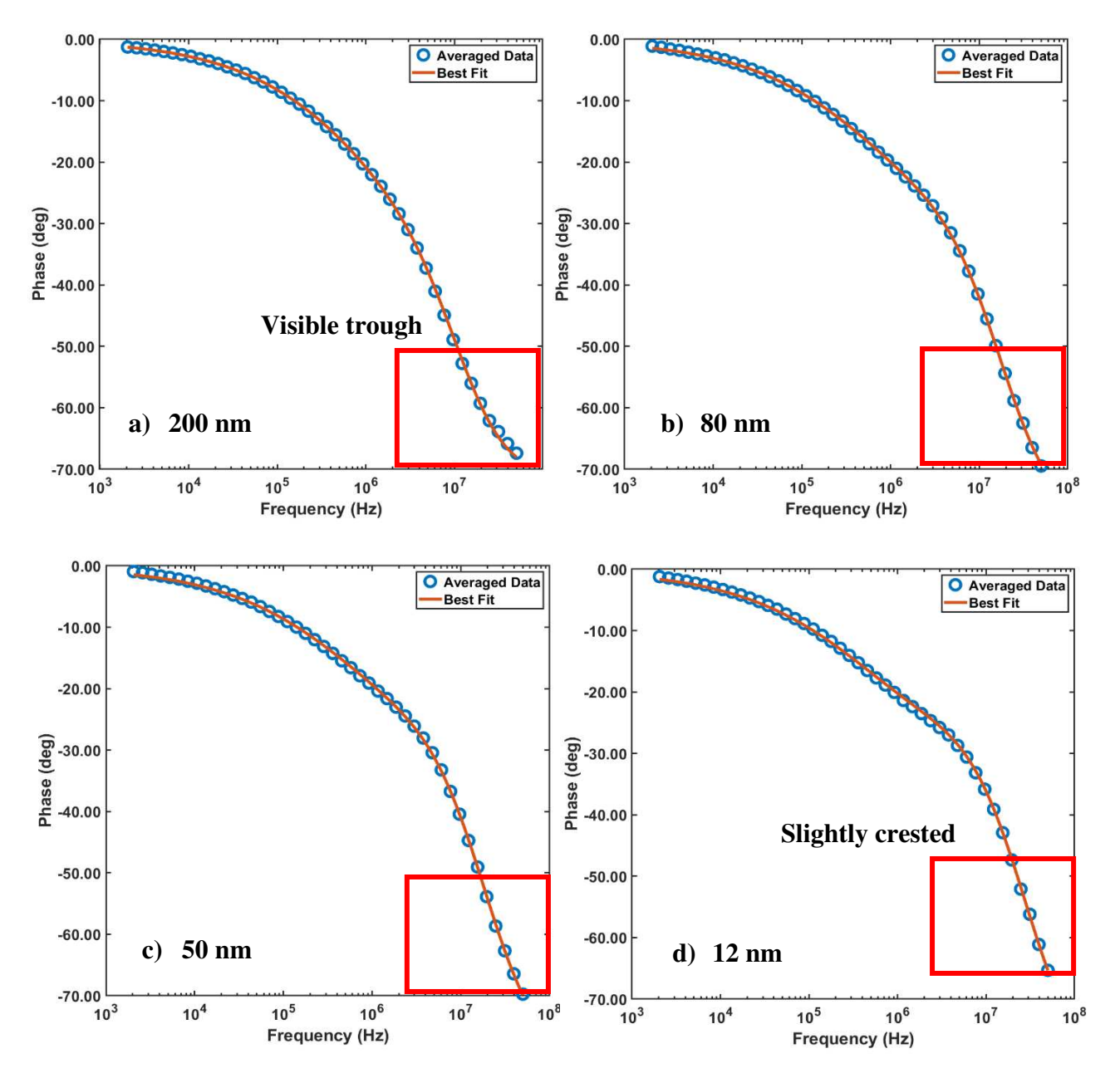


FIG 6. Curve fitting analysis for STO thin films of varying thickness a) 200 nm b) 80 nm c) 50 nm d) 12 nm, determining the thermal properties of the STO films under examination

In Figs. 7 a, b, c, d, shows the sensitivity of the parameters across the modulation frequency range. The measurement is found to be sensitive to cross-plane thermal conductivity (TC), with the extent of sensitivity remaining relatively constant in all the cases. This is an indication that the values of cross-plane conductivity obtained by the curve fitting analysis will be accurate. We also observe that the solution is relatively insensitive to the thermal boundary conductance (TBC) G_1 and G_2 in all the cases. Therefore, we assign a high value to G_1 and G_2 equal to $1000 \,\mathrm{MWm^{-2}K^{-1}}$ and consider them to be fixed input parameters with a known value, for our analysis. This clears up the fact that there is little to no resistance to heat flow across these thermal boundaries and the effective PLEASE CITE THIS ARTICLE AS DOI: 10.1116/6.0003320 resistance to the heat flow comes predominantly from the material's thermal conductivity. In this analysis we also consider the anisotropy $(k_{\parallel} / k_{\perp})$ as 1, implying that the materials are isotropic. Under this imposed isotropic condition, the analysis software outputs the thermal conductivity value (either the cross-plane or in-plane) based on the measurement's sensitivity to

This leaves us with only 2 unknown parameters, namely, STO cross-plane thermal conductivity and laser spot size. The reason we fit the spot size along with the thermal conductivity for our analysis is because the main source of experimental uncertainty comes from the estimation of spot size^{50,51}.

the specific parameter. In our case, the system is sensitive to the cross-plane thermal conductivity

of the STO thin films and is insensitive to the in-plane thermal conductivity. Hence, by keeping

the anisotropy to be 1 (essentially not decoupling) the cross and the in-plane thermal

conductivities), we reduce another fitting parameter, aiding us in the fitting analysis.

This spot size can be determined in two ways, by using a knife edge method with a x-y piezo stage and by using Gaussian beam optics with a stationary sample stage. The knife edge method is an

PLEASE CITE THIS ARTICLE AS DOI: 10.1116/6.0003320

expensive method of determining spot size, as it requires a specially prepared knife-edge sample, a piezo stage and additional photodetectors, attached to the stage⁵².

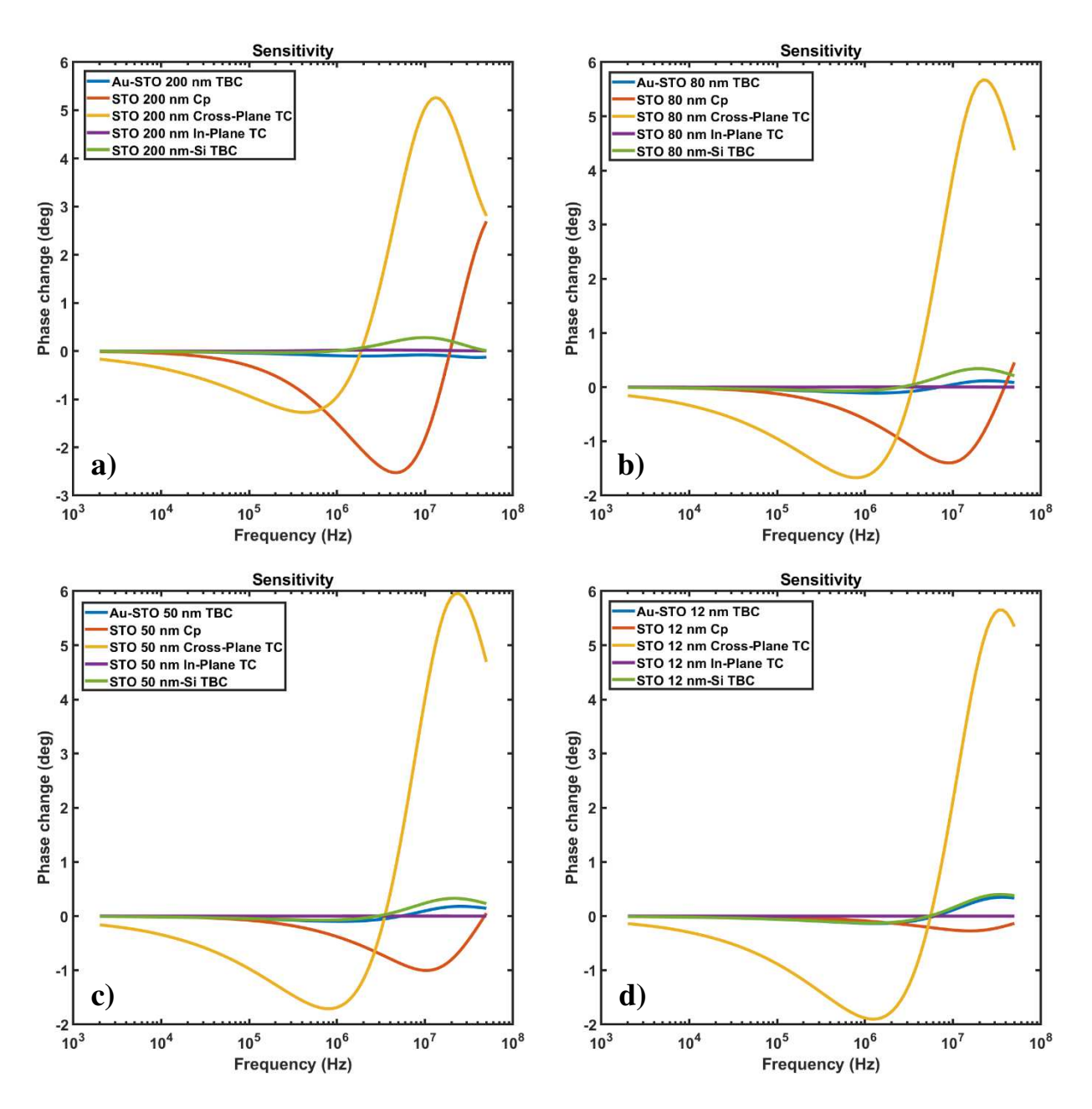


FIG 7. Sensitivity plots for different parameters for STO thin films of varying thickness a) 200nm b) 80nm c) 50nm d) 12nm, indicating the extent to which each parameter is sensitive to the measurement done at each thickness. Sensitivity of every parameter is measured across the modulation freq.

PLEASE CITE THIS ARTICLE AS DOI: 10.1116/6.0003320

One can reduce the expense of spot size measurement, with a stationary stage, which would be less accurate. In this method, the pump laser spot is scanned over the probe layer spot, generating a Gaussian spot intensity profile, which is fitted to a calculated Gaussian spot intensity profile. This is done in both x and y directions. The curve fit analysis of these intensity plots provides us with a reasonable estimation of the spot size, at the cost of increased uncertainty.

Hence, for our analysis, a 2-parameter was essential to perform thermal conductivity measurements accurately. Thin films can generally show anisotropic nature due to their very small thickness, but when we analyze the sensitivity plots, we see that there is no sensitivity to the inplane thermal conductivity property in any of the samples. This is because the substrate in use is Si ($C_P = 1.64 \text{ MJm}^{-3}\text{K}^{-1}$, used in the fitting of STO measurements), which has a very high thermal conductivity value of ~145 Wm⁻¹K⁻¹ (also used in the fitting analysis). This leads to quick dissipation of the heat into the Si substrate, diminishing the spreading of the heat in the radial direction, leading to insensitivity to the in-plane thermal conductivity. We then perform a 2-parameter fit for the cross-plane thermal conductivity of STO and laser spot size, to find the best fit solution for the material systems with varying thickness. The values of STO thermal conductivity for different thicknesses are tabulated in Table. 2.

The value of thermal conductivity for STO thin film decreases with the decreasing thickness of the thin film. The reduction in the thermal conductivity across various thicknesses ranges from \sim 38% to 93%, when compared to the value of bulk single crystal of STO, purchased from MTI Corporation⁵³. The thermal conductivity of bulk single crystal was also measured in our FDTR system, with a value of 12.5 Wm⁻¹K⁻¹. The approach for its analysis was like the one used in the case of thin films. These k values have an uncertainty of 10%, 11%, 11% and 13% respectively, from the thickest to the thinnest film.

PLEASE CITE THIS ARTICLE AS DOI: 10.1116/6.0003320

The 38% reduction in thermal conductivity value of 200 nm thin film relative to bulk sample is due to both finite-size effects associated with scattering of phonons at boundaries of the STO sample as well as due to presence of dislocations in the sample. Epitaxial films of STO on Si have dislocations due to the mismatch of not just the in-plane but also out-of-plane lattice constants between STO and Si. Steps on the Si surface associated with the miscut in the wafer are incommensurate in height relative to the lattice constant of STO.

Consequently, even very thin films, such as the 12 nm thick film studied here, have dislocations that give rise to anti-phase boundaries in the STO⁵⁴. At present, the effect of such dislocations on thermal conductivity is not well established. We estimate the distance between dislocations to be ~ 25 nm in our films⁵⁵. The even larger 93% decrease in the thermal conductivity value of the 12 nm thick film relative to the bulk sample, points to reduction in part from finite-size effects, as the density of dislocations due to steps on the Si surface in the 12 nm thick film and the 200 nm thick film are comparable.

TABLE II. Thickness dependent thermal conductivity of STO thin films on Si

STO thin film thickness	k (Wm ⁻¹ K ⁻¹)
200 nm	7.4±0.74
80 nm	3.86±0.43
50 nm	2.35±0.26
12 nm	0.8±0.1

B. Volumetric heat capacity (C_p) estimation

PLEASE CITE THIS ARTICLE AS DOI: 10.1116/6.0003320

Figs. 7 a, b, c, and d show a steady reduction in measurement's sensitivity to the volumetric heat capacity (C_p) of STO, with decreasing thickness. To measure C_p , we need to apply a 3-parameter curve fit analysis, with parameters being fitted as C_p , k, and thickness. Table. 3 shows that the value of C_p is most certain for the 200 nm thick sample. Although the value of uncertainty increases with the decreasing thickness of the films, the C_p values seem to be relatively in the range of the literature values. The uncertainty values are associated to the parameter's sensitivity across the film thicknesses, as seen in Fig. 7. Therefore, to accurately measure the volumetric heat capacity and to be confident in the value derived from analysis using FDTR, the film needs to be thick enough for it to be sensitive to C_p . The measured C_p values for the thickest film is 3.07 MJm⁻³K⁻¹ with an uncertainty of 6%.

The reason why the 3-parameter fit worked in this case is that phase lag sensitivities of cross-plane thermal conductivity and C_p shows us that they traverse a completely different trend, across the range of modulation frequencies of pump laser (2000 Hz – 50 MHz), and the fact that there is a sensitivity difference between the two parameters at the lowest frequency.

TABLE III. Volumetric heat capacity for STO at different thickness with their uncertainties

STO thin film thickness	$C_p (10^6 \mathrm{Jm^{\text{-}3}K^{\text{-}1}})$	Uncertainty (%)	
200 nm	3.07	6	
80 nm	2.79	21	
50 nm	2.71	35	
12 nm	2.64	51	

Conclusions:

PLEASE CITE THIS ARTICLE AS DOI: 10.1116/6.0003320

Journal of Vacuum



In summary, we measured the thermal properties of STO thin films on Si substrate for four different thicknesses of STO films, 200nm, 80 nm, 50 nm and 12nm as well as a bulk STO sample. The thermal conductivity values were measured to be 7.4, 3.86, 2.35 and 0.8 W m⁻¹K⁻¹ for the 200 nm, 80 nm, 50 nm and 12 nm, respectively. The k value for the bulk STO sample was measured to be at 12.5 Wm⁻¹K⁻¹. A significant reduction of 93% in the thermal conductivity value was observed for 12 nm thin film, in comparison to the value of bulk single crystal STO. The percentage reduction in k values of different thickness thin films indicate the approximate mean free path of phonons. A 38% reduction in thermal conductivity for the 200 nm thick sample, relative to bulk value, indicates that phonons with mean free path larger than 200 nm, contribute ~38% to overall thermal conductivity. The measurements were sensitive to the cross-plane thermal conductivity of the thin films and volumetric heat capacity (C_p) but were insensitive to other parameters such as the in-plane thermal conductivity and thermal boundary conductance. The measured values of C_p of the thin films were in reasonable agreement with the literature values. A co-relation between uncertainty of C_p values across the samples and the measurement's sensitivity to the parameter was found. Sample's decreasing thickness leads to decreased sensitivity to C_p , which is responsible for the increasing uncertainty, with it being the highest for the thinnest sample. The work provides understanding of thickness dependence of thermal conductivity of STO on Si substrate.

Conflicts of Interest

There are no conflicts of interest to declare.

Acknowledgements

RSA, RM, FT, SD, AN, and JG acknowledge support from National Science Foundation award under Award No. #2115067. JHN and MC acknowledge support from the National Science Foundation under Award No.'s CMMI-2132105, and DMR-1508530.

This is the author's peer reviewed, accepted manuscript. However, the online version of record will be different from this version once it has been copyedited and typeset.

PLEASE CITE THIS ARTICLE AS DOI: 10.1116/6.0003320

Data Availability Statement:

The data that support the findings of this study are available from the corresponding author upon reasonable request.

References:

- ¹ C. Yu, M.L. Scullin, M. Huijben, R. Ramesh, and A. Majumdar, Appl. Phys. Lett. **92**(19), 191911 (2008).
- ² A.O. Fumega, Y. Fu, V. Pardo, and D.J. Singh, Phys. Rev. Mater. **4**(3), 033606 (2020).
- ³ C.M. Brooks, R.B. Wilson, A. Schäfer, J.A. Mundy, M.E. Holtz, D.A. Muller, J. Schubert, D.G. Cahill, and D.G. Schlom, Appl. Phys. Lett. **107**(5), 051902 (2015).
- ⁴ M. Imada, A. Fujimori, and Y. Tokura, Rev. Mod. Phys. **70**(4), 1039–1263 (1998).
- ⁵ J.M.D. Coey, M. Viret, and S. Von Molnar, Adv. Phys. **48**(2), 167–293 (1999).
- ⁶ M. Dawber, K.M. Rabe, and J.F. Scott, Rev. Mod. Phys. **77**(4), 1083 (2005).
- ⁷ T. Ohnishi, M. Lippmaa, T. Yamamoto, S. Meguro, and H. Koinuma, Appl. Phys. Lett. **87**(24), (2005).
- ⁸ N. Nakagawa, H.Y. Hwang, and D.A. Muller, Nat. Mater. **5**(3), 204–209 (2006).
- ⁹ M. Varela, S.D. Findlay, A.R. Lupini, H.M. Christen, A.Y. Borisevich, N. Dellby, O.L.

Krivanek, P.D. Nellist, M.P. Oxley, and L.J. Allen, Phys. Rev. Lett. 92(9), 095502 (2004).

- ¹⁰ M. Lippmaa, N. Nakagawa, M. Kawasaki, S. Ohashi, and H. Koinuma, Appl. Phys. Lett. **76**(17), 2439–2441 (2000).
- ¹¹ R. Vassen, X. Cao, F. Tietz, D. Basu, and D. Stöver, J. Am. Ceram. **83**(8), 2023–2028 (2000).
- ¹² J.W. Fergus, J. Eur. Ceram. **32**(3), 525–540 (2012).
- ¹³ A. Weidenkaff, R. Robert, M. Aguirre, L. Bocher, T. Lippert, and S. Canulescu, Renew. Ener. **33**(2), 342–347 (2008).

This is the author's peer reviewed, accepted manuscript. However, the online version of record will be different from this version once it has been copyedited and typeset.

PLEASE CITE THIS ARTICLE AS DOI: 10.1116/6.0003320

- ¹⁴ J. Sun, and D.J. Singh, APL Mater. **4**(10), 104803 (2016).
- ¹⁵ X.-L. Shi, H. Wu, Q. Liu, W. Zhou, S. Lu, Z. Shao, M. Dargusch, and Z.-G. Chen, Nano Energy 78, 105195 (2020).
- ¹⁶ P.-Y. Lesaicherre, H. Yamaguchi, Y. Miyasaka, H. Watanabe, H. Ono, and M. Yoshida, Integr. Ferroelectr. **8**(1–2), 201–225 (1995).
- ¹⁷ M. Kiyotoshi, and K. Eguchi, Appl. Phys. Lett. **67**(17), 2468–2470 (1995).
- ¹⁸ G.D. Wilk, R.M. Wallace, and J. Anthony, J. of Appl. Phys. **89**(10), 5243–5275 (2001).
- ¹⁹ D.S. Shin, S.T. Park, H.S. Choi, I.H. Choi, and J.Y. Lee, Thin Solid Films **354**(1–2), 251–255 (1999).
- ²⁰ J. Qiao, and C.Y. Yang, Mater. Sci. Eng. R Rep. **14**(4), 157–201 (1995).
- ²¹ M. Leskelä, H. Mölsä, and L. Niinistö, Supercond. Sci. Technol. **6**(9), 627 (1993).
- ²² J.A. Seijas-Bellido, C. Escorihuela-Sayalero, M. Royo, M.P. Ljungberg, J.C. Wojdeł, J. Íñiguez, and R. Rurali, Phys. Rev. B **96**(14), 140101 (2017).
- ²³ M. Royo, C. Escorihuela-Sayalero, J. Íñiguez, and R. Rurali, Phys. Rev. Mater. **1**(5), 051402 (2017).
- ²⁴ J.F. Ihlefeld, B.M. Foley, D.A. Scrymgeour, J.R. Michael, B.B. McKenzie, D.L. Medlin, M. Wallace, S. Trolier-McKinstry, and P.E. Hopkins, Nano Lett. **15**(3), 1791–1795 (2015).
- ²⁵ P.E. Hopkins, C. Adamo, L. Ye, B.D. Huey, S.R. Lee, D.G. Schlom, and J.F. Ihlefeld, Appl. Phys. Lett. **102**(12), (2013).
- ²⁶ S. Ning, S.C. Huberman, C. Zhang, Z. Zhang, G. Chen, and C.A. Ross, Phys. Rev. Appl. **8**(5), 054049 (2017).
- ²⁷ E. Langenberg, D. Saha, M.E. Holtz, J.-J. Wang, D. Bugallo, E. Ferreiro-Vila, H. Paik, I. Hanke, S. Ganschow, and D.A. Muller, Nano Lett. **19**(11), 7901–7907 (2019).

PLEASE CITE THIS ARTICLE AS DOI: 10.1116/6.0003320

- ²⁸ P. Torres, J. Íñiguez, and R. Rurali, Phys. Rev. Lett. **123**(18), 185901 (2019).
- ²⁹ D.-W. Oh, J. Ravichandran, C.-W. Liang, W. Siemons, B. Jalan, C.M. Brooks, M. Huijben,
- D.G. Schlom, S. Stemmer, and L.W. Martin, Appl. Phys. Lett. 98(22), (2011).
- ³⁰ A. Sarantopoulos, D. Saha, W.-L. Ong, C. Magén, J.A. Malen, and F. Rivadulla, Phys. Rev. Mater. **4**(5), 054002 (2020).
- ³¹ T. Katsufuji, T. Saiki, S. Okubo, Y. Katayama, and K. Ueno, Phys. Rev. Mater. **2**(5), 051002 (2018).
- ³² D. Bugallo, E. Langenberg, E. Carbó-Argibay, N. Varela Dominguez, A.O. Fumega, V. Pardo,
- I. Lucas, L. Morellón, and F. Rivadulla, J. Phys. Chem. Lett. **12**(49), 11878–11885 (2021).
- ³³ S.S. Kumar, A.Z. Barasheed, and H.N. Alshareef, ACS Appl. Mater. **5**(15), 7268–7273 (2013).
- ³⁴ B.M. Foley, H.J. Brown-Shaklee, J.C. Duda, R. Cheaito, B.J. Gibbons, D. Medlin, J.F. Ihlefeld, and P.E. Hopkins, Appl. Phys. Lett. **101**(23), (2012).
- ³⁵ E. Breckenfeld, R. Wilson, J. Karthik, A.R. Damodaran, D.G. Cahill, and L.W. Martin, Chem. Mater. **24**(2), 331–337 (2012).
- ³⁶ L. Zhang, N. Li, H.-Q. Wang, Y. Zhang, F. Ren, X.-X. Liao, Y.-P. Li, X.-D. Wang, Z. Huang, and Y. Dai, Chin. Phys. B **26**(1), 016602 (2017).
- ³⁷ S. Wiedigen, T. Kramer, M. Feuchter, I. Knorr, N. Nee, J. Hoffmann, M. Kamlah, C.A. Volkert, and C. Jooss, Appl. Phys. Lett. **100**(6), (2012).
- ³⁸ V. Martelli, J.L. Jiménez, M. Continentino, E. Baggio-Saitovitch, and K. Behnia, Phys. Rev. Lett. **120**(12), 125901 (2018).
- ³⁹ R.A. McKee, F.J. Walker, and M.F. Chisholm, Phys. Rev. Lett. **81**(14), 3014–3017 (1998).
- ⁴⁰ D.P. Kumah, J.H. Ngai, and L. Kornblum, Adv. Funct. Mater. **30**(18), 1901597 (2020).

PLEASE CITE THIS ARTICLE AS DOI: 10.1116/6.0003320

- ⁴¹ Z.H. Lim, N.F. Quackenbush, A.N. Penn, M. Chrysler, M. Bowden, Z. Zhu, J.M. Ablett, T.-L. Lee, J.M. LeBeau, J.C. Woicik, P.V. Sushko, S.A. Chambers, and J.H. Ngai, Phys. Rev. Lett.
- ⁴² P. Jiang, X. Oian, and R. Yang, J. Appl. Phys. **124**(16), (2018).

123(2), 026805 (2019).

- ⁴³ P. Jiang, X. Qian, and R. Yang, Rev. Sci. Instrum. **89**(9), (2018).
- ⁴⁴ J. Yang, C. Maragliano, and A.J. Schmidt, Rev. of Sci. Instrum. **84**(10), (2013).
- ⁴⁵ R. Muthaiah, R.S. Annam, F. Tarannum, A.K. Gupta, J. Garg, and S. Arafin, Phys. Chem. Chem. Phys. **24**(47), 28814–28824 (2022).
- ⁴⁶ M.G. Pamato, I.G. Wood, D.P. Dobson, S.A. Hunt, and L. Vočadlo, J. Appl. Cryst. **51**(2), 470–480 (2018).
- ⁴⁷ J.P. Coughlin, and R.L. Orr, J. Am. Chem. Soc. **75**(3), 530–531 (1953).
- ⁴⁸ D. de Ligny, and P. Richet, Phys. Rev. B **53**(6), 3013 (1996).
- ⁴⁹ E. McCalla, M.N. Gastiasoro, G. Cassuto, R.M. Fernandes, and C. Leighton, Phys. Rev. Mater. **3**(2), 022001 (2019).
- ⁵⁰ J.A. Malen, K. Baheti, T. Tong, Y. Zhao, J.A. Hudgings, and A. Majumdar, J. of Heat Transfer **133**(081601), (2011).
- ⁵¹ A.J. Schmidt, R. Cheaito, and M. Chiesa, Rev. Sci. Instrum. **80**(9), 094901 (2009).
- ⁵² J. Yang, Thermal Property Measurement with Frequency Domain Thermoreflectance, Boston University, 2016.
- ⁵³"MTI Corp Leading provider of lab equipments and advanced crystal substrates," (n.d.).
- ⁵⁴ X. Shen, K. Ahmadi-Majlan, J.H. Ngai, D. Wu, and D. Su, Appl. Phys. Lett. **106**(3), 032903 (2015).

Journal of Vacuum Science & Technology A



This is the author's peer reviewed, accepted manuscript. However, the online version of record will be different from this version once it has been copyedited and typeset.

PLEASE CITE THIS ARTICLE AS DOI: 10.1116/6.0003320

⁵⁵ M. Chrysler, J. Gabel, T.-L. Lee, A.N. Penn, B.E. Matthews, D.M. Kepaptsoglou, Q.M.

Ramasse, J.R. Paudel, R.K. Sah, J.D. Grassi, Z. Zhu, A.X. Gray, J.M. LeBeau, S.R. Spurgeon,

S.A. Chambers, P.V. Sushko, and J.H. Ngai, Phys. Rev. Mater. 5(10), 104603 (2021).